

Cite this: DOI:[10.56748/ejse.23536](https://doi.org/10.56748/ejse.23536)Received Date: 18 October 2023
Accepted Date: 19 February 2024

1443-9255

<https://ejsei.com/ejse>Copyright: © The Author(s).
Published by Electronic Journals
for Science and Engineering
International (EJSEI).
This is an open access article
under the CC BY license.<https://creativecommons.org/licenses/by/4.0/>

Research on the mechanics differences between single-row and double-row side piles of station using the PBA method

Xingkai Pei ^a, Jing Sun ^a, Guangyao Guo ^{b*}, Xuemin Zhou ^b, Shuai Zhang ^b^a Guangzhou Metro Design and Research Institute Co., Ltd., Guangzhou, 510010, China.^b Southwest Jiaotong University, Key Laboratory of Transportation Tunnel Engineering, Ministry of Education, Chengdu, No. 111, North Section, Second Ring Road, Jinniu District, 610031, China.*Corresponding author: 595826005@qq.com

Abstract

The side pile is a crucial mechanical component in station construction using the PBA (pile-beam-arch) method, and its stability during the construction process cannot be overstated. The mechanical differences between single-row and double-row side piles in this construction method have garnered significant attention, yet few studies have been conducted on this matter. Therefore, this paper employs numerical simulation to compare the deformation and mechanical properties of single-row and double-row side piles (the adopted pile type is micro steel pipe pile, abbreviated as MSPP) in a metro station using the PBA method. The findings are validated through the model experiment. It is found that the soil arch effect created by the front-row pile of the double-row piles serves as the primary lining, offering a certain shielding effect to the soil stress behind the back-row pile. Notably, the soil stress values in double-row pile conditions are slightly higher compared to single-row pile condition, leading to a noticeably smaller final deformation of the pile top. The combined bending moments and axial forces of the front-row and back-row piles in double-row piles exceed those of a single-row pile. Specifically, bending moments are highest in single-row piles, followed by front-row piles and then back-row piles, while axial forces are highest in single-row piles, followed by back-row piles and then front-row piles. This suggests that the bending moments and axial forces of double-row piles are smaller than those of a single-row pile. The internal force distribution within the double-row pile is more balanced, thereby enhancing the lining strength and improving the station's safety through the PBA method. The findings in this paper can serve as valuable references for the design and construction of similar projects.

Keywords

PBA method, MSPP, Mechanical differences, Deformation characteristics, Soil arch effect

1. Introduction

With the rapid urbanization process, numerous metro stations are being constructed in cities to accommodate the increasing transportation needs of the population (Sun et al. 2023; Zhang et al. 2023). As these stations are primarily situated in bustling urban areas, their excavation and construction can result in the deformation of the overlying strata. Therefore, it is very important to choose an appropriate metro construction method to reduce the interference to the existing building facilities (Liu et al. 2018). The PBA method is a metro construction method that has gradually emerged in recent years. This method has the advantages of significant control of surface subsidence, flexible structural form, and small impact on surrounding buildings. It has gradually become an important choice in metro construction (Wang et al. 2012; Wang et al. 2021; Li 2022). During the construction period of the station, the side pile is an important component in this kind of lining system (Zeng et al. 2022; Li et al. 2023). The side pile transmits the load of the upper soil to the deep soil and is vital in limiting the deformation of the station. The previous research on metro stations with PBA method mostly focused on the control of surface settlement and the optimization of the excavation method (Wang and Guo 2016; Yu et al. 2019; Li and Chen 2020; Guo et al. 2021; Lv et al. 2023). On the other hand, there are few studies on the design and mechanical effects of the side piles of the station with PBA method at home and abroad. Most of them focus on the installation of piles in the reinforcement of composite foundations, lining of foundation pits, construction of roadbed engineering, and so on (Liu and Li 2012; Lai et al. 2014; Cheng et al. 2021; Wang 2021; Zhu et al. 2023; Zhang et al. 2023). Given the unique force transmission mechanism of the side pile employed in the station with PBA method, it is imperative to avoid simply adopting previous results and to conduct further research. Typically, single-row piles are utilized as side piles, while double-row piles may be employed to meet the force requirements of the station when using the PBA method. This approach can lead to increased construction costs and complexity. Therefore, during the design phase of station projects, it is essential to thoroughly consider the appropriate use of single-row and double-row pile options. However, current research lacks comprehensive studies on

the differences in supporting mechanics between single-row and double-row pile configurations in stations with the PBA method.

Therefore, this study focuses on a metro station project in Guangzhou that employs the PBA method. Utilizing numerical simulation, it examines the differences in lining effects between single-row and double-row piles within this station. The calculated results are further validated through model testing. The goal of this research is to provide valuable guidance for the selection of pile rows in similar stations utilizing the PBA method during the design and construction stages.

2. Project Overview

A metro station in Guangzhou is constructed by PBA method, and the station is a two-story underground structure. The height of the station is 17.8m and the width is 21.7m. The buried depth of the station structure is about 9m, and the cross-section of the structure is displayed in Fig. 1. According to the engineering geological survey report and the exposure of the rock stratum in the field construction, the station is mainly located in the strongly weathered rock stratum, and the geotechnical engineering properties are poor, as displayed in Fig. 2.

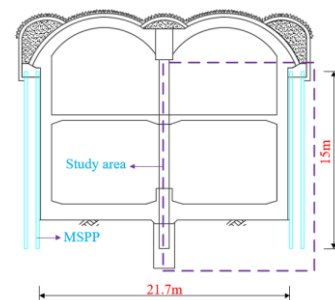


Fig. 1 Cross-section of the station



Fig. 2 Site rock disclosure map

Because the clearance size of the first pilot tunnel of the station is only 5.0m × 4.4m (height × width), the working space of the side piles in the pilot tunnel is narrow, which is not conducive to the construction of large

pile foundations. Therefore, in the early design stage of side piles, it is planned to use MSPP with small pile-forming machines, simple and efficient construction, and good pile-forming quality as the selection of side piles for the PBA method. The side pile size is diameter \times wall thickness \times length = 273 mm \times 12mm \times 15m, and the embedded depth of side pile is 2.5m.

3. Numerical calculation instructions

3.1 Simulation model

The numerical calculation is conducted through FLAC3D. The relevant physical parameters and geometric parameters of the simulation model are taken according to the field data of the project. The numerical analysis model is displayed in Fig. 3 (a). Note: the side piles are inside the “purple region” due to display issues. To guarantee the accuracy of the numerical analysis as well as reduce the impact of the boundary effects on the calculation results, the model width is 36 m, the height is 25m, and the longitudinal length is 21m. The corresponding normal displacement constraints are set to the bottom and surrounding boundary of the model (Zhao et al. 2022). The load boundary is applied to the top to simulate the actual buried depth of the project. To reduce calculation difficulty, the top arch load F is decomposed into horizontal load (F_x) and vertical load (F_y). Based on the actual engineering parameters, the bedded-beam model is used to calculate the F_x and F_y . The obtained value is as follows: $F_x=800\text{kN/m}$ and $F_y=1200\text{kN/m}$, and the soil pressure q on the soil behind the piles is 250kPa. The specific simulation boundary conditions are shown in Fig. 3 (b).

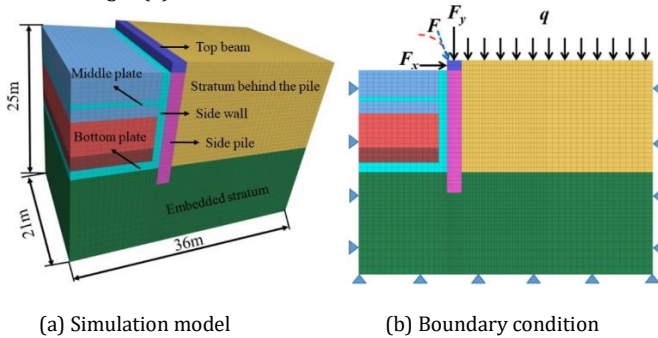


Fig. 3 Numerical calculation model

3.2 Calculation parameters

The surrounding rock and the lining structure of the station are simulated by solid elements. The surrounding rock adopts the ideal elastic-plastic constitutive model and obeys the Mohr-Coulomb strength yield criterion (Lim and Ou 2017). The supporting structure is regarded as a linear elastic material, and the elastic constitutive model is adopted. The simulation parameter of the surrounding rock as well as the lining structure is displayed in Table 1. The side pile structures of the station through the PBA method are simulated by the pile structure unit. The interaction between the piles and the soil can be realized by the coupling connecting springs at each node of the pile unit. The force and deformation are transmitted by the normal and tangential coupling springs. By referring to relevant literatures (Luo et al. 2007; Chen and Xu 2013), plenty of FLAC3D simulation tests, and verified through the test results. Then the coupling spring parameter of the pile element in this paper is obtained, as shown in Table 2.

Table 1 Calculation parameters

Category	Name	Material	Density ρ /(kg/m^3)	Elastic modulus E /MPa	Poisson ratio μ	Cohesion c /kPa	Friction angle φ / $^\circ$
Surrounding rock	Stratum behind the pile	Strongly weathered rock stratum	2100	120	0.33	50	28
	Embedded stratum	Slightly weathered rock stratum	2600	2000	0.25	260	32
Lining structure	Top beam	C30 concrete	2500	30000	0.20	-	-
	Middle plate	C35 concrete	2700	31500	0.20	-	-
	Bottom plate	C35 concrete	2700	31500	0.20	-	-

Table 2 Calculation parameters of the side pile

Elastic modulus /GPa	Tangential coupling spring			Normal coupling spring		
	Rigidity /Pa \cdot m $^{-1}$	Cohesion /Pa	Friction angle / $^\circ$	Rigidity /Pa \cdot m $^{-1}$	Cohesion /Pa	Friction angle / $^\circ$
60.0	4.0×10^8	4.0×10^4	22.4	4.0×10^8	4.0×10^4	22.4

3.3 Arrangement of the measuring points

To deeply compare the force as well as deformation properties of single-row and double-row side piles and the evolution law of soil pressure on the pile side, the side pile in the middle of the station is selected for analysis. At the same time, it also decreases the impact of boundary conditions on the simulation results. Monitoring points are set every 1.25m along the pile depth direction to monitor and extract the lateral deformation and internal force of the whole monitored pile. The schematic diagrams of the position of the monitored side pile and the monitored points are shown in Fig. 4.

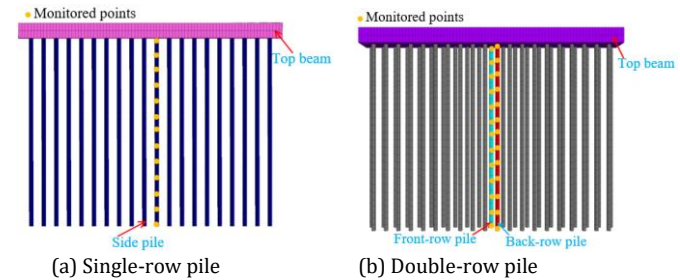


Fig. 4 Schematic diagram of the monitored pile and monitored points.

3.4 Simulation of the construction stages

In the numerical simulation of the PBA method, the construction of side piles is realized by building pile structure units. The excavation process of the station is realized by setting corresponding solid units as empty units. The construction of the top beam, middle plate, bottom plate, and other structures is realized by assigning corresponding support parameters to solid units. The construction process of the metro station with the PBA method is conducted through the following procedures, and detailed simulation steps are shown in Fig. 5.

- The side pile and top beam are installed; the buckle load (F_x and F_y) of the arch structure is applied to the top beam and q_{soil} is applied;
- The first soil layer in the main body of the station is excavated;
- The middle plate and the upper side wall structure are installed, and the second soil layer of the main body of the station is excavated;
- The third soil layer of the main body of the station is excavated, and the bottom plate, bottom longitudinal beam, and lower side wall are installed, and the construction of the main structure of the station is completed.

4. Result analysis

4.1 Mechanical properties of the soil behind piles

To gain a deeper understanding of the stress evolution in the soil behind the pile during the various construction stages of the metro station, we've utilized the PBA method, focusing specifically on the single-row side pile. Through this analysis, we've delved into the X-direction stress distribution characteristics at different soil depths and construction stages, which are clearly outlined in Figs. 6~7. Note: section 1 and section 2 refer to the depth of -2.50 m and -7.50 m from the pile top, respectively.

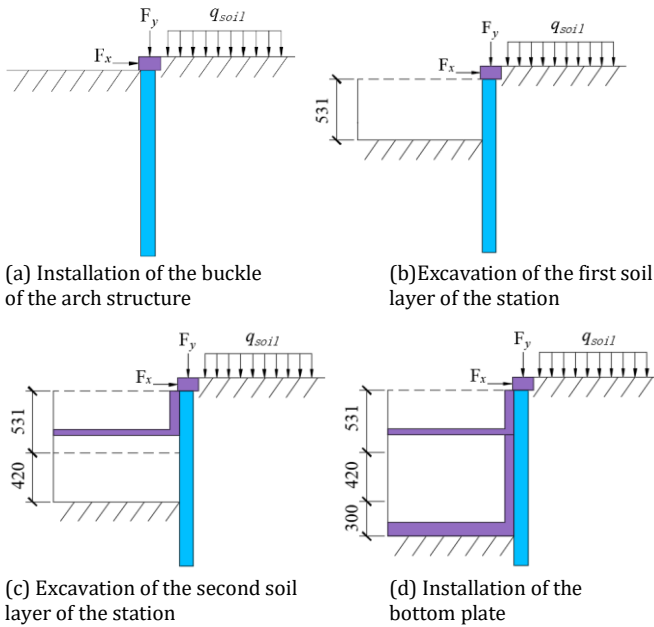


Fig. 5 The main construction steps of PBA numerical simulation /cm

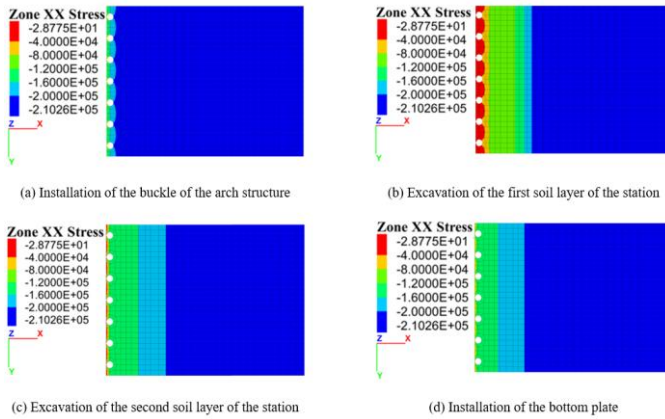


Fig. 6 Stress cloud diagram in the X direction of soil under single-row piles of side piles (Section 1)

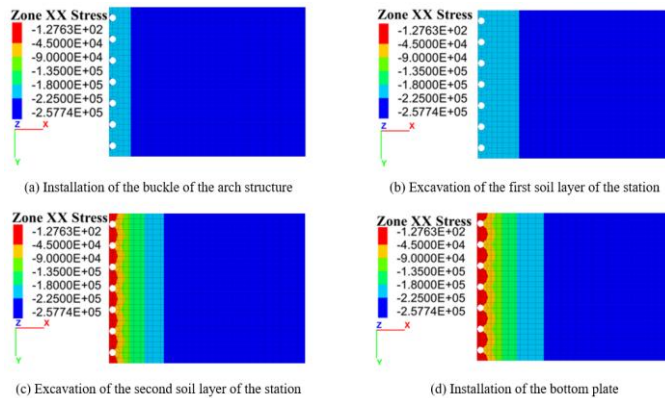


Fig. 7 Stress cloud diagram in the X-direction of soil under single-row piles of side pile (Section 2)

In Figs. 6~7, at the depth of -2.50m from the pile top, there is a certain stress concentration in the soil behind the pile after the completion of the arch construction. The side pile actively displaces the soil behind it due to the arching forces at its top. This compression squeezes the soil, prompting it to resist deformation and generate passive soil pressure. Consequently, the X-direction stresses within the soil behind the pile are greater than those found between the piles, ultimately creating an active soil arching stress circle. At the depth of -7.50m from the pile top, the soil is less disturbed due to the distance from the pile top, and the stress is almost linearly distributed without obvious change. When excavating the first soil layer of the station, the soil behind the pile is deformed, which squeezes the side pile structure and produces active earth pressure. There is an obvious arch stress zone near the side pile structure at a depth of -2.50m near the excavation surface. In addition, there is also a red stress dissipation zone in the soil between piles. The stress in the X-direction of

the soil in this range attenuates rapidly. A yellow arch stress concentration zone appears on the back of the pile, and the soil stress deflects. This part of the soil transfers the soil pressure after the arch to the side pile structure through the arch foot, indicating that an effective soil arching effect is formed here. With the construction process of the station, the excavation surface of the soil continues to move down, the soil arch effect of the soil behind the pile also shifts downward, and the soil arching effect of the shallow soil gradually disappears. The soil arching effect between side piles becomes evident at a depth of -7.50m from the pile top following the excavation of the station soil. This observation suggests that the development, growth, and collapse of the soil arching effect between piles is intricately linked to the construction process. The evolution law of soil stress behind double-row side piles with the construction process is basically the same as that of single-row side piles, which is no longer repeated here.

To more intuitively compare the difference of soil arching effect formed by single-row and double-row side piles, the X-direction stress distribution law of deep soil after the completion of the bottom plate is extracted and analyzed, as shown in Fig. 8.

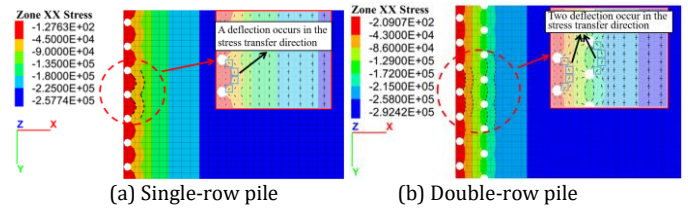


Fig. 8 X-direction stress distribution of the soil under single-row pile as well as double-row pile

In Fig.8, whether it is a single-row side pile or a double-row side pile, the soil between piles forms a certain soil arch effect. The soil stress undergoes deflection towards the soil arch structure area, subsequently traveling along its trace towards the side pile structure. This indicates that the soil arch structure area effectively shields the soil between the piles, ensuring that the side pile structure bears most of the soil stress. Conversely, the soil within the stress dissipation area experiences minimal stress from the external soil. However, from the X-direction overall stress size and distribution pattern of the two, the soil stress value under the double-row side pile condition is slightly greater than that under the single-row pile condition. The stress arch axis distribution of the former is denser than that of the latter, indicating that the supporting effect of the former is better. On the other hand, in the case of double-row side piles, the front-row pile and the back-row pile have blocking effects on the soil behind the pile. The stress transfer direction of the soil behind the pile deflects twice to the pile body. So, there are two rows of arched stress bands, that is, there is a double-layer soil arching effect. Because the front-row piles in the double-row piles are closer to the free face of the station excavation, they are only subjected to the force of the soil between the two rows of piles. The pressure difference between the front and rear sides of the piles is large, and the stress dissipation area between the piles is more obvious. However, the combined effect of the soil between the two rows of piles and the soil behind them results in minimal changes in the stress value of the soil between the piles. Consequently, the soil arching effect observed between the back-row piles is not as prominent as that observed in the front-row. At this juncture, the soil arching effects created by the front-row piles of the double-row piles assume a pivotal role in providing lining support. Conversely, the soil arching effect of the back-row pile serves to partially mitigate the stress within the soil behind the pile, exercising a certain shielding influence.

4.2 Deformation properties of the pile body

The evolution curve of the lateral displacement of the single-row pile, as well as double-row pile with the construction process, is shown in Fig. 9. Note: for the convenience of the description in figure, the main construction stage is abbreviated: stage A is the stage that the buckle arch is completed, stage B is the stage that the first soil layer is excavated, stage C is the stage that the second soil layer is excavated, and stage D is the stage that the installation of bottom plate is completed. The comparison diagram of the lateral displacement and reduction rate of single-row piles and double-row piles after the completion of the station construction is shown in Fig. 10.

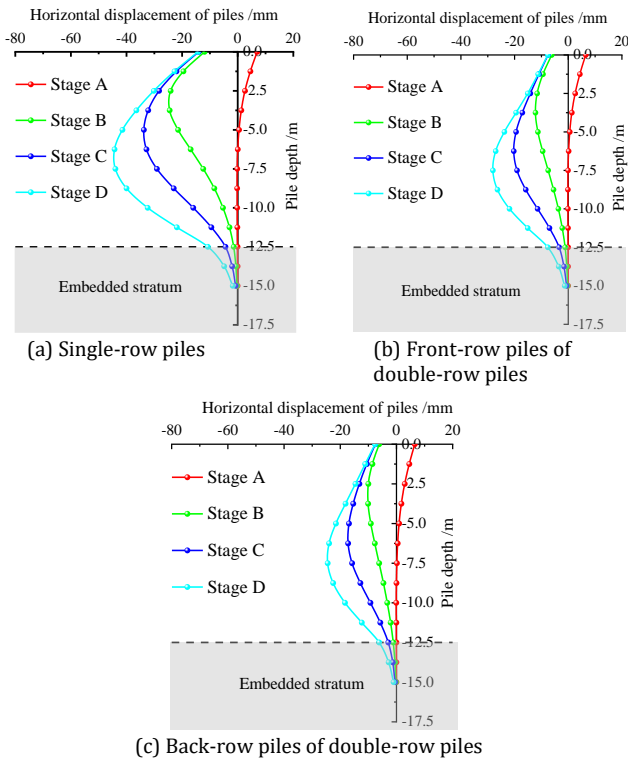


Fig. 9 Lateral displacements of side pile body change with the construction process

In Fig. 9, after the completion of the buckle arch, the side pile is similar to the cantilever beam structure, the forward positive displacement is generated to the outside of the station under the action of the load force of the pile top. The lateral displacement of the pile top position is the largest, and the displacement value can reach 7mm. Subsequently, because of the unloading effect caused by the continuous downward construction of the soil within the station, the pile body gradually shifts towards the interior of the station, exhibiting a characteristic belly-expansion deformation, featuring a larger middle and smaller ends. The lateral displacements of the pile top of the side pile structure change most sharply in the excavation of the first soil layer of the station, and the change value can reach 18.9mm (namely, from 7mm to -11.9mm). The lateral displacements of the pile top in this construction stage should be paid attention to. If necessary, certain lateral lining measures can be taken to the pile top structure to ensure the stability of the side pile structure.

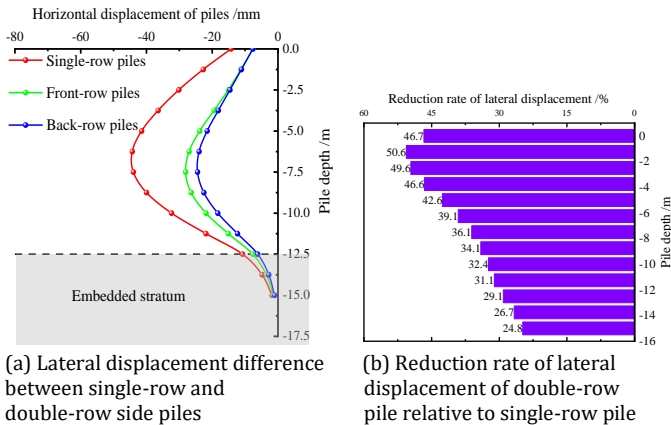


Fig. 10 Comparison of the final lateral displacement of single-row and double-row side piles along the pile depth

In Fig. 10, the final lateral deformation of single-row piles as well as double-row piles is characterized by belly expansion type deformation with large at the middle and small at both ends and the largest lateral displacement occurs in the middle of the monitored pile. The lateral displacement of the single-row pile is significantly larger than that of the double-row piles. The maximum lateral displacement in the single-row pile is -44.29mm, while the maximum lateral displacements of the front-row pile as well as back-row piles in the double-row piles are -28.07 mm and -24.45 mm, respectively. Compared with the maximum lateral displacement of a single-row pile, the largest lateral displacement of a double-row pile is reduced by 16.22mm. Besides, it shows that the double-row pile can significantly reduce the horizontal displacement of the side pile, especially above the middle of the side pile, and the largest reduction rate of displacement even reaches 50.6%. The reason lies in the fact that

the double-row pile structure, connected by a crown beam at the pile top, forms an integral lining system. This system effectively harnesses the lining capacity of both the front-row and back-row piles, as well as the soil between them, thereby enhancing the overall stiffness of the structural system. The single-row pile simply relies on its pile stiffness and the soil resistance at the embedded end to resist the soil pressure behind the pile. So, the supporting stiffness of the double-row pile structure is larger than that of the single-row piles, and the lateral displacement of the pile body is also significantly smaller.

In addition, due to the synergistic deformation of the crown beam at the pile top, the lateral displacement deformation of the front-row piles as well as the back-row piles at the pile top is basically equal. With the increase of the buried depth of the pile, because the front-row piles are closer to the excavation side of the station soil, the soil pressure differences between the inside and outside of side piles are greater than that of the back-row piles. Under the action of the soil pressure behind the pile, the horizontal deformation of front-row piles is larger than that of the back-row piles. Therefore, the lateral deformation of the side pile structure ranges as single-row piles > front-row piles > back-row piles, and the side pile structure near the excavation side of the station is more worthy of attention.

The final vertical settlement and lateral displacements of the side piles at the pile top after the completion of the station construction are shown in Fig. 11.

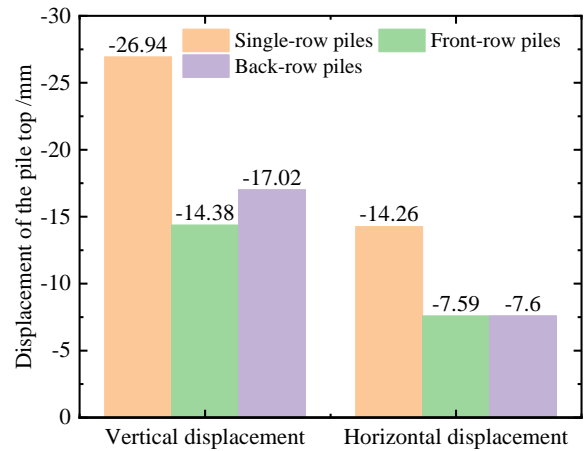


Fig. 11 Final displacements of the side pile top

In Fig. 11, the final deformations of the pile top of the double-row pile structure are significantly smaller than that of the single-row piles, which also shows that the double-row piles significantly improve the lining strength. Compared with the front-row pile in the double-row pile at the same position, the vertical settlement of the pile top is reduced from -26.94mm to -14.38mm, and the horizontal displacement is reduced from -14.26mm to -7.59mm, with a decrease of 46.62% and 46.77%, respectively. This suggests that when a row of lining pile structures is added to the backside of single-row piles, the additional back-row pile can exert a certain shielding effect on the front-row piles, sharing a portion of the vertical load at the pile top and the soil stress behind it. This distribution of load results in a reduction in the deformation of the front-row pile. The back-row pile as well as front-row pile jointly improve the vertical carrying capacities as well as the lateral bending deformations resistance of the overall structure of the side piles.

4.3 Mechanical properties of the side piles

The evolution curves of internal forces of the side piles with the construction process are shown in Figs. 12~13, and the internal force comparison diagram of the single-row pile and double-row pile after the completion of the station construction is shown in Fig. 14.

In Figs. 12~13, with the excavation of the station soil, the bending moments of the side pile gradually increase, and the position of the section of the largest bending moments gradually develops downward with the downward movement of the soil excavation surface. The bending moments of the side pile are mainly in the form of large in the middle and small at both ends. The side piles above the excavation face of the soil are mainly pulled by the excavation side of the station. The pile embedded in the lower rock layer is opposite due to the embedding effect. The axial force of the side pile presents a broken line distribution characteristic of large at the upper side and small at the lower side. The axial forces gradually increase with the excavation of the station soil, and the change is the most severe when the first soil layer is excavated. This is primarily due to the excavation of the station soil, resulting in partial looseness around the pile caused by construction disturbances. Consequently, the side friction resistances of the side piles are significantly reduced, leading to an increase in axial forces within the side piles.

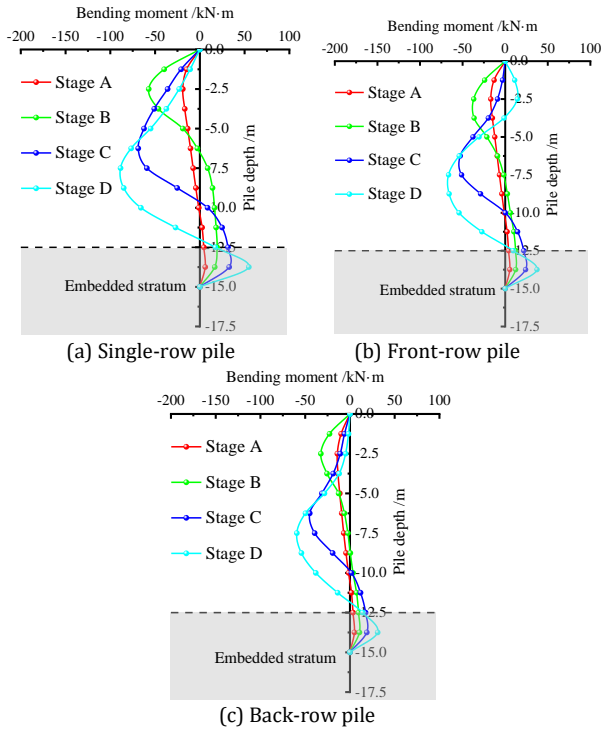


Fig. 12 Distribution rule of the bending moment of the pile body

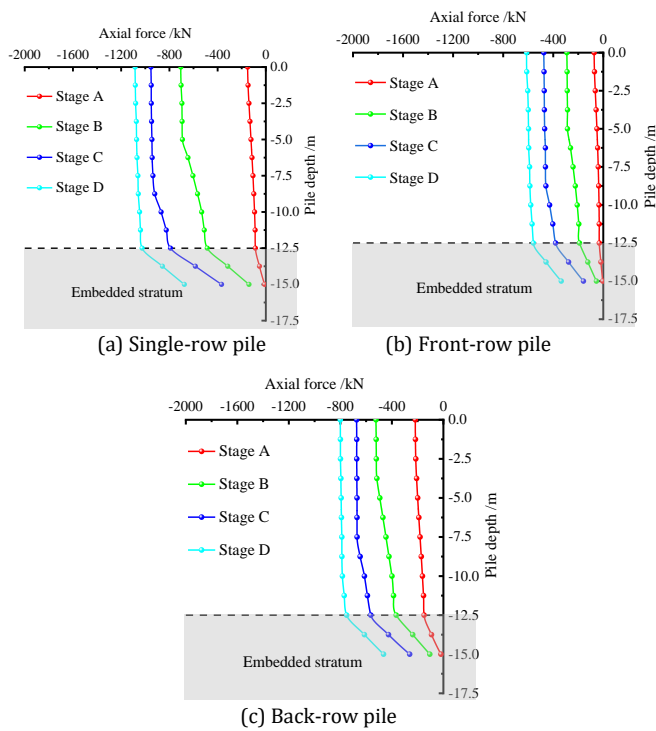


Fig. 13 Distribution law of axial forces of the pile body

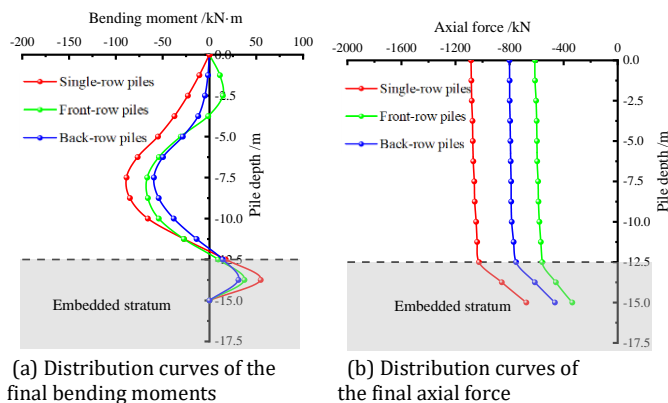


Fig. 14 Final internal force comparison curve of side pile structure

In Fig. 14, the final bending moments of single-row piles as well as double-row piles are still dominated by the bow distribution characteristics of large in the middle and small at both ends. The bending moment distribution of single-row piles is significantly larger than that of double-row piles, and the internal force deformation distribution of the pile body has a slight upward trend. The bending moments of the side piles are ranged as single-row piles > front-row piles > back-row piles. The maximum bending moment of single-row piles is -88.51kN·m. The largest bending moments in the front-row pile as well as the back-row pile in the double-row pile are -66.48kN·m and -59.30kN·m, respectively, and the bending moment of front-row piles is 24.89% lower than that of the single-row piles.

Furthermore, the front-row pile within the double-row pile configuration experiences a positive bending moment of inner compression and outer tension at both the top and bottom of the pile. Conversely, the single-row pile and the back-row pile exhibit a positive bending moment of inner compression and outer tension solely at the embedded end of the pile bottom. It is conjectured that the back-row piles exert a shielding effect on the front-row piles, sharing a significant portion of the soil pressure behind the piles. Consequently, the lateral lining forces on the middle plate structure of the front-row pile are larger than the soil pressure borne directly by the piles. This imbalance results in an inflection bending phenomenon at the pile top of the side pile structure.

As far as the axial force distribution of the pile body is concerned, the axial forces of the pile body of the single-row piles as well as the double-row piles are characterized by a broken line distribution. The axial forces of the side pile are ranged as single-row piles > back-row piles > front-row piles, and the maximum axial force of single-row piles is -1084.26kN. The maximum axial forces of the front-row pile as well as the back-row pile in the double-row piles are -612.42kN and -800.53kN, respectively, which are different from the distributing law of the bending moments. As the back-row piles are positioned closer to the center of the crown beam than the front-row pile, the eccentricity of the vertical load on the buckle arch is reduced. Consequently, the back-row pile experiences less impact from eccentric loads compared to the front-row pile. This results in a larger vertical load borne by the back-row piles, leading to an increase in axial forces within the pile body and a decrease in bending moments.

4.4 Verification of the numerical model

To further verify the rationality of the simulation results in this paper, it is necessary to compare them with the experimental results. One of the authors of this paper (Zhang 2023) carried out a model experiment (for the single-row side pile case) with the same construction process as the simulation calculation with a similarity ratio of 30. The stratum and component parameters as well as the applied load values are strictly converted according to the similarity ratio. The specific derivation and experimental process are not mentioned in detail here because of page limitations, more information can be referred to the literature (Zhang 2023). The picture of the experiment is shown in Fig. 15. F_x is applied through jack I; F_y is applied through jack II; the soil pressure behind the pile (q_{soil}) is applied through jack III. The comparison of the final bending moment of the side pile between the numerical simulation and the experiment after conversion through the similarity ratio is shown in Fig. 16. It can be seen from Fig. 16 that the bending moment curves obtained by experiment method and simulation method both show the distribution characteristics of large in the middle and small at both ends. And the trend and value of the curves are very close to each other, which verifies the rationality of the numerical calculation in this paper.

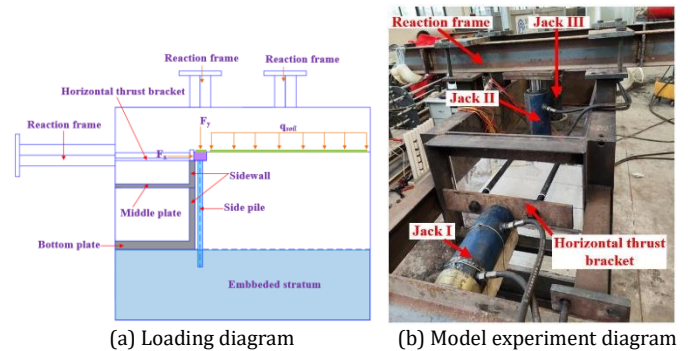


Fig. 15 Loading device for the model experiment

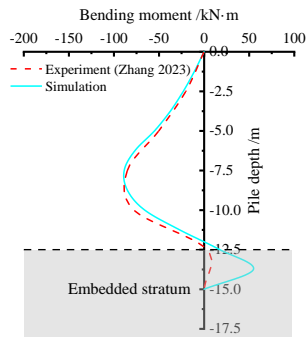


Fig. 16 Comparison of the bending moment between model experiment and numerical simulation

5. Conclusion

1. In the case of double-row side piles, the soil arch effect between the pile of the back-row piles is not as significant as that of the front-row piles. At this time, the soil arch effect formed by the front-row piles of double-row piles plays a main lining role. The soil arching effect of back-row piles partially blocks and weakens the soil pressure behind the pile and plays a certain shielding effect.
2. In the double-row side pile condition, the soil stress value is slightly higher than that of the single-row pile condition. The stress arch axis distribution of the double-row side pile is denser, resulting in significantly smaller final deformation of the pile top. These findings suggest that the double-row side piles significantly enhance the lining strength.
3. The bending moments of side pile structure are ordered as "single-row piles > front-row piles > back-row piles". The sum of the bending moment of the front-row piles as well as the back-row piles in the double-row piles is significantly larger than the largest bending moments of the single-row piles. Compared with the single-row piles, the bending moment value of front-row piles with the largest bending moments in the double-row piles is reduced by 24.89%. In contrast to the single-row piles, the distribution rules of the bending moments of the double-row piles are more reasonable, which can effectively improve structural stability.
4. The axial forces of side piles exhibit a gradient, with the single-row piles experiencing the highest forces, followed by the back-row piles and then the front-row piles. This pattern differs from the distribution law of bending moments, which exhibits a different trend. This is because the back-row piles are closer to the center of the crown beam, the eccentricity of the vertical load of the buckle arch is smaller, and the shared vertical load is larger, leading to greater axial forces of the pile body as well as the smaller bending moments of the pile body.

Acknowledgments

This work was supported by the Research Project on the Key Technology of Station with PBA Method (GL-2022-B-438) and the research and development project Ministry of Housing and Urban-Rural Development of the People's Republic of China (2022-K-044).

Conflicts of interest

The authors declare that there are no conflicts of interest regarding the publication of this paper.

Data Availability

The data that appeared in this paper will be available upon reasonable request.

Reference

Cheng, X.S., Gong, L.J., Liu, G.N. 2021. Bearing capacity characteristics and differential settlement of composite foundation with column-hammered and thrust-expanded piles. *International Journal of Geomechanics*, 21(9): 04021164. [https://doi.org/10.1061/\(ASCE\)GM.1943-5622.0002050](https://doi.org/10.1061/(ASCE)GM.1943-5622.0002050)

Chen, Y.M., Xu, D.P. 2013. *FLAC/FLAC3D foundation and engineering application*. China Water and Power Press, Beijing. (in Chinese).

Guo, X.Y., Wang, Z.Z., Geng, P., Chen, C.J., Zhang, J. 2021. Ground surface settlement response to metro station construction activities using pile-beam-arch method. *Tunnelling and Underground Space Technology*, 108: 103729. <https://doi.org/10.1016/j.tust.2020.103729>

Luo, W.L., Liu, C.W., Han, X. 2007. Numerical simulation of behaviour of piled foundation influenced by tunneling. *Rock and Soil Mechanics*, 28: 403-407. (in Chinese) <https://doi.org/10.16285/j.rsm.2007.s1.131>

Liu, J.Z., Sun, L.C., Zhang, Z., Xu, H., Ding, G.P. 2018. Study on mechanical effect of PBA Method in metro station. *Chinese Journal of Underground Space and Engineering*, 14(S1): 240-247. (in Chinese).

Li, T., Li, Y., Yang, T.Y., Hou, R., Gao, Y., Liu, B., Qiao, G.G. 2023. Influence of the large-span pile-beam-arch construction method on the surface deformation of a metro station in the silty clay-pebble composite stratum. *Materials*, 16(7): 2934. <https://doi.org/10.3390/ma16072934>

Lv, J.B., Lu, J.J., Wu, H. 2023. Study on the mechanical characteristics and ground surface settlement influence of the rise-span ratio of the pile-beam-arch method. *Applied Sciences*, 13(9): 5678. <https://doi.org/10.3390/app13095678>

Li, C.J. 2022. Research on adaptability of PBA improved construction method for underground station in loess area. *Railway Standard Design*, 66(6): 97-104. (in Chinese) <https://doi.org/10.13238/j.issn.1004-2954.202102190006>

Lai, H.J., Zheng, J.J., Zhang, J. 2014. DEM analysis of "soil"-arching within geogrid-reinforced and unreinforced pile-supported embankments. *Computers and Geotechnics*, 61: 13-23. <https://doi.org/10.1016/j.compgeo.2014.04.007>

Li, J.K., Chen, P. 2020. Comparative analysis of group cave effect in construction of metro station by pile-beam-arch (PBA) method. *Science Technology and Engineering*, 20(14): 5737-5742. (in Chinese). <https://doi.org/10.3969/j.issn.1671-1815.2020.14.042>

Liu, X.L., Li, B. 2012. Analysis of supporting mechanism of micro-steel-pipe piles in rock foundation pit. *Rock and Soil Mechanics*, 33(S1): 217-222. (in Chinese). <https://doi.org/10.16285/j.rsm.2012.s1.035>

Lim, A., Ou, C.Y. 2017. Stress paths in deep excavations under undrained conditions and its influence on deformation analysis. *Tunnelling and Underground Space Technology*, 63: 118-132. <https://doi.org/10.1016/j.tust.2016.12.013>

Sun, J., Pei, X.K., Yang, C., Zhu, B.Z. 2023. Dynamic response analysis of the process of the utility shield tunnel under-passing the operating subway tunnel. *Electronic Journal of Structural Engineering*, 23(3): 44-52. <https://doi.org/10.56748/ejse.234433>

Wang, T., Luo, F.R., Liu, W.N., Li, X.G. 2012. Study of surface settlement and flexible joint pipeline deformation induced by metro station construction with PBA method. *China Civil Engineering Journal*, 45(2): 155-161. (in Chinese). <https://doi.org/10.15951/j.tmgxcb.2012.02.005>

Wang, X.Y., Lei, K., Wang, T., Zhang, J.G. 2021. Prediction of existing pipeline settlement resulting from the construction of an underground metro station using the pile-beam-arch (PBA) method. *China Civil Engineering Journal*, 54(S1): 65-75. (in Chinese). <https://doi.org/10.15951/j.tmgxcb.2021.s1.005>

Wang, Z.Z., Guo, X.Y. 2016. Research on ground settlement of metro station construction by PBA method. *Journal of Dalian University of Technology*, 56(3): 257-262. (in Chinese). <https://doi.org/10.7511/dllgxb201603006>

Wang, X.Y. 2021. Application research on deep collapsible loess foundation treatment by gravel pile. *Chinese Journal of Underground Space and Engineering*, 17(4): 1164-1170. (in Chinese)

Yu, L., Zhang, D.L., Fang, Q., Cao, L.Q., Xu, T., Li, Q.Q. 2019. Surface settlement of metro station construction using pile-beam-arch approach. *Tunnelling and Underground Space Technology*, 90: 340-356. <https://doi.org/10.1016/j.tust.2019.05.016>

Zeng, Y., Bai, Y., Zou, Y., Huang, B. 2022. Numerical study on stratigraphic and structural deformation patterns considering surface load with pile-beam-arch method construction. *Symmetry*, 14(9): 1892. <https://doi.org/10.3390/sym14091892>

Zhao, J.P., Tan, Z.S., Yu, R.S., Li, Z.L., Zhang, X.R., Zhu, P.C. 2022. Deformation responses of the foundation pit construction of the urban metro station: a case study in Xiamen. *Tunnelling and Underground Space Technology*, 128: 104662. <https://doi.org/10.1016/j.tust.2022.104662>

Zhu, W.W., Xi, Y., Liu, B.T., Liu, Y., Yang, K., Li, Z., Yang, X., Wang, B.Y. 2023. Monitoring and discussion on distribution mode of earth pressure behind piles under the pile-supporting system in a deep foundation pit. *Building Structure*, 53(17): 134-140. (in Chinese). <https://doi.org/10.19701/j.jzjz.lz.210218>

Zhang, S. 2023. Study on the selection and construction mechanical behavior of side pile in metro station using pile-beam-arch method. Master's thesis, Southwest Jiaotong University.

Zhang, H.J., Liu, G.N., Liu, W.X., Zhang, S., Chen, Z.K. 2023. Mechanical evolution law and deformation characteristics of preliminary lining about newly built subway tunnel closely undercrossing the existing station: A case study. *Geomechanics and Engineering*, 35(5), 525-538. <https://doi.org/10.12989/gae.2023.35.5.525>

Zhang, D.S., Zhang, X.L., Tang, H.T., Zhao, Z.Q., Guo, J., Zhao, H.H. 2023. Effects of soil arching on behavior of composite pile supporting foundation pit. *Computational Particle Mechanics*, 10: 645-662. <https://doi.org/10.1007/s40571-022-00518-1>